Tidal field anisotropy as a tracer of cosmic voids

Sebastian Bustamante $\star$[1], Jaime E. Forero-Romero[2]

[1] *Instituto de Física - FCEN, Universidad de Antioquia, Calle 67 No. 53-108, Medellín, Colombia*
[2] *Departamento de Física, Universidad de los Andes, Cra. 1 No. 18A-10, Edificio Ip, Bogotá, Colombia*

10 January 2015

ABSTRACT
Finding and characterizing underdense regions (voids) in the large scale structure of the Universe is an important task in cosmological studies. In this paper we present a novel approach to find voids in cosmological simulations. Our approach is based on algorithms that use the tidal and the velocity shear tensors to locally define the cosmic web. Voids are identified using the fractional anisotropy (FA) computed from the eigenvalues of each web scheme. We define the void boundaries using a watershed transform based on the local minima of the FA and its boundaries as the regions where the FA is maximized This void identification technique does not have any free parameters and does not make any assumption on the shape or structure of the voids. We test the method on the Bolshoi simulation and report on the density and velo ity profiles for the voids found using this new scheme.

Key words: Cosmology: theory - large-scale structure of Universe - Methods: data analysis - numerical - N-body simulations

1 INTRODUCTION

Since voids were found in the first compiled galaxy surveys they have been identified as one of the most striking features of the Cosmic Web (Chincarini & Rood 1975; Gregory & Thompson 1978; Einasto et al. 1980a,b; Kirshner et al. 1981; Zeldovich et al. 1982; Kirshner et al. 1987; Bond et al. 1996). However, due to the large volume extension of void regions ($\sim 5 - 10$ Mpch^{-1}), statistically meaningful catalogs of voids (Pan et al. 2012; Sutter et al. 2012; Nadathur & Hotchkiss 2014) have only become available through modern galaxy surveys like the two-degree field Galaxy Redshift Survey (Colless et al. 2001, 2003) and the Sloan Digital Sky Survey (York et al. 2000; Abazajian et al. 2003). This advancement generated a great interest to study voids observationally during the last decade (Hoyle & Vogeley 2004; Croton & et al. 2004; Rojas et al. 2005; Ceccarelli et al. 2006; Patiri et al. 2006; Tikhonov 2006; Patiri et al. 2006; Tikhonov 2007; von Benda-Beckmann & Müller 2008; Foster & Nelson 2009; Ceccarelli et al. 2013; Sutter et al. 2014).

On the theoretical side the rough theoretical framework that explains the origin of voids was established in the seminal work of Zel'dovich (1970) and refined in the following decades. The first detailed theoretical models describing formation, dynamics and properties of voids (Hoffman & Shaham 1982; Icke 1984; Bertschinger 1985; Blumenthal et al. 1992) were complemented and extended by numerical stud-

ies (Martel & Wasserman 1990; Regos & Geller 1991; van de Weygaert & van Kampen 1993; Dubinski et al. 1993; Bond et al. 1996). Currently, the dominant tendency to study voids relies on using data from N-body simulations. For an extensive compilation of previous numerical works we refer the reader to Colberg et al. (2008).

The relevance of voids to cosmological studies can be summarized in three aspects (Platen et al. 2007). First, voids are a key ingredient of the Cosmic Web. They dominate the volume distribution at large-scales and additionally, they compensate overdense structures in the total budget of matter. Second, voids provide a valuable resource for inferring and probing cosmological parameters as their structure and dynamics are highly determined by these values. Third, they are a largely a largely pristine environment to test galaxy evolution.

Although a visual recognition of voids in galaxy surveys and simulations is possible in most cases, a formal systematic identification is desirable for statistical studies. However, the community does not have an unambiguous definition of cosmic voids. There are nany different void finding techniques in the literature (for a detailed comparison of different schemes, see the Void Finder Comparison Project Colberg et al. (2008)). In spite of the diversity of existing schemes, they can be roughly classified into two main types. First, geometric schemes based on point spatial or redshift distribution of galaxies in surveys or dark matter halos in simulations (Kauffmann & Fairall 1991; Müller et al. 2000; Gottlöber et al. 2003; Hoyle & Vogeley 2004; Brunino et al.

$\star$ sebastian.bustamante@udea.edu.co

2007; Foster & Nelson 2009; Micheletti & et al. 2014; Sutter et al. 2014); second, schemes based on the smooth and continuous matter density field either from simulations or from reconstruction procedures on surveys (Plionis & Basilakos 2002; Colberg et al. 2005; Shandarin et al. 2006; Platen et al. 2007; Neyrinck 2008; Muñoz-Cuartas et al. 2011; Neyrinck et al. 2013; Ricciardelli et al. 2013).

Here we introduce a new tracer of the structure of cosmic voids that can be used once the continous matter density or velocity distribution is known. The algorithm is based on two tensorial schemes used to classify the cosmic web. The first (the T-web) is based on the Hessian of the gravitational potential or tidal tensor (Hahn et al. 2007; Forero-Romero et al. 2009). The second (the V-web) is based on the velocity shear tensor (Hoffman et al. 2012). These web schemes classify the Cosmic Web into four different types of environment depending on the counting of the number of eigenvalues below an user-defined threshold (λ_{rmth}): voids, sheets, filaments and knots for $3, 2, 1$ or 0 eigenvalues below λ_{th}, respectively.

This procedure allows a new description of the internal structure of voids that goes beyond a simple definition of a void as just an underdense regions in the large-scale matter distribution. The tidal and the shear tensors encode more information than the density field as they trace the collapsing or expanding nature of the matter field, which defines the dynamics of the Cosmic Web.

The tracer that we use to define the voids is the fractional anisotropy (FA) computed from the set of eigenvalues of the tensor under consideration. The FA was initially introduced by Basser (1995) to quantify the anisotropy degree of the diffusivity of water molecules through cerebral tissue in nuclear magnetic resonance imaging. Libeskind et al. (2013) introduced this concept in the context of Cosmic Web classification schemes.

Once we establish the FA as a void tracer, we proceed to identify individual voids as basins of local minima. For this we implement a *watershed transform algorithm* (Beucher & Lantuejoul 1979; Beucher & Meyer 1993) which has been used to define as catching basins of local minima of the density field (Platen et al. 2007; Neyrinck 2008); we use insted minima of the FA field to find define the voids.

This paper is organized as follows. In Section 2 we describe the algorithms we use to find the cosmic web in N-body simulations. Then in Section 4 we explain in detail our void finder based on the fractional anisotropy of the tidal and shear tensor fields. In Section **??** we describe the numerical experiments we perform to show the performance of the new void finding technique. Our results are presented in 5 to finally comment and conclude about these findings in Section 6.

2   ALGORITHMS TO LABEL THE COSMIC WEB

2.1   The tidal web (Tweb)

This scheme was initially proposed by Hahn et al. (2007) as an alternative for classifying the Cosmic Web based on the tidal tensor. The tidal tensor allows a classification in terms of the orbital dinamics of the matter field This approach extends to second-order the equations of motion around local minima of the gravitational potential. The second-order term corresponds to the tidal tensor, which is defined as the Hessian matrix of the normalized gravitational potential.

$$T_{\alpha\beta} = \frac{\partial^2 \phi}{\partial x_\alpha \partial x_\beta}, \tag{1}$$

where the physical gravitational potential has been rescaled by a factor of $4\pi G\bar{\rho}$ in such a way that ϕ satisfies the following Poisson equation

$$\nabla^2 \phi = \delta, \tag{2}$$

with $\bar{\rho}$ the average density in the Universe, G the gravitational constant and δ the dimensionless matter overdensity.

Since the tidal tensor can be represented by a real and symmetric 3×3 matrix, it is always possible to diagonalize it and obtain three real eigenvalues $\lambda_1 \geqslant \lambda_2 \geqslant \lambda_3$ with its corresponding eigenvectors $\mathbf{u}_1, \mathbf{u}_2, \mathbf{u}_3$. This set of eigenvalues are indicators of the local orbital stability in each direction $\mathbf{u}_i$, which is to label the Cosmic Web. The number of positive (stable) or negative (unstable) eigenvalues allows to label a location into one of the next four types of environment: voids (3 negatives eigenvalues), sheets (2), filaments (1) and knots (0). A modification to this scheme was introduced by Forero-Romero et al. (2009) by means of a relaxation of the stability criterion. The relative strength of each eigenvalue is no longer defined by the sign, but instead by a threshold value λ_{th} that can be tuned in such a way that the visual impression of the web-like matter distribution is reproduced.

2.2   The velocity web (Vweb)

We also use a kinematic scheme to define the Cosmic Web environment in the simulation, which has been thoroughly described in Hoffman et al. (2012). This scheme has been used to study the shape, spin and peculiar velocity alignments of dark matter halos with the cosmic web (Libeskind et al. 2013; Forero-Romero et al. 2014). We refer the reader to these papers to find a detailed description of the algorithm, its limitations and capabilities. The Vweb scheme for environment finding is based on the local velocity shear tensor calculated from the smoothed dark matter velocity field in the simulation. This tensor is given by the following expression

$$\Sigma_{\alpha\beta} = -\frac{1}{2H_0} \left(\frac{\partial v_\alpha}{\partial x_\beta} + \frac{\partial v_\beta}{\partial x_\alpha} \right), \tag{3}$$

where v_α and x_α represent the α component of the comoving velocity and position, respectively. Like the tidal tensor, $\Sigma_{\alpha\beta}$ can be represented by a 3×3 symmetric matrix with real values, making it possible to find three real eigenvalues and its corresponding eigenvectors.

In this case we also use the relative strength of the three eigenvalues with respect to a threshold value λ_{th} to classify the cosmic web in the four web types we have already described.

Usually, the threshold is a free parameter that is tuned to reproduce the visual appearence of the comic web. In this paper we take a different approach. We find the optimal

value of the threshold based on the maximization of the fractional anisotropy field in the locations label as filaments and walls.

3 NUMERICAL SIMULATIONS

We use the Bolshoi simulation to test the method describe in the paper. This simulation follows the non-linear evolution of a dark matter density field on a cubic volume of size $250h^{-1}$Mpc sampled with 2048^3 particles. The cosmological parameters in the simulation are $\Omega_m = 0.27$, $\Omega_\Lambda = 0.73$, $h = 0.70$, $n = 0.95$ and $\sigma_8 = 0.82$ for the matter density, cosmological constant, dimensionless Hubble parameter, spectral index of primordial density perturbations and normalization for the power spectrum, respectively. This values are consistent with the seventh year of data of the Wilkinson Microwave Anisotropy Probe (WMAP) (Jarosik et al. 2011). For more detailed technical information about the simulation, see Klypin et al. (2011).

We find the cosmic web we estimate first the density and velocity fields using a *cloud-in-cell* (`CIC`) algorithm onto a grid of 256^3 cells, corresponding to a spatial resolution of $0.98h^{-1}$Mpc per cell side. These fields are smoothed with a gaussian filter with a width of $\sigma = 0.98h^{-1}$Mpc . We compute the tidal and shear tensors through finite-differences and Finally, the eigenvalues and eigenvectors of the tensor are obtained for each grid cell. The data we use here is publicly available through the MultiDark database `http://www.multidark.org/MultiDark/` which is described in Riebe et al. (2013).

4 A NEW VOID FINDING TECHNIQUE

4.1 The fractional anisotropy

The fractional anisotropy (FA), as developed by Basser (1995), was conceived to quantify the anisotropy degree of a diffusion process, e.g. the diffusivity of water molecules through cerebral tissue in nuclear magnetic resonance imaging. Here we propose the FA, much in the same way as Libeskind et al. (2013), as a tracer of cosmic voids.

The FA is defined as follows.

$$\text{FA} = \frac{1}{\sqrt{3}} \sqrt{\frac{(\lambda_1 - \lambda_3)^2 + (\lambda_2 - \lambda_3)^2 + (\lambda_1 - \lambda_2)^2}{\lambda_1^2 + \lambda_2^2 + \lambda_3^2}}, \quad (4)$$

where the eigenvalues are taken from either the Tweb or the Vweb (FA-Tweb and FA-Vweb respectively). Such as it is defined, FA$= 0$ corresponds to an isotropic distribution ($\lambda_1 = \lambda_2 = \lambda_3$) and FA$= 1$ with a highly anisotropic distribution.

In left panels of Fig. 1 we show the FA field for both web schemes over a slide of the simulation. From this Figure we can observe that both, voids and knots, display a highly isotropic expanding dynamic at their centres, becoming gradually more anisotropic at outer regions. On the other hand the filamentary structure is traced by high FA values. These characteristics are the key to use the FA as a tracer of cosmic voids.

4.2 Fractional anisotropy as a void tracer

Voids are regions where $\lambda_3 \leqslant \lambda_2 \leqslant \lambda_1 \leqslant \lambda_{th}$. This implies that a void is completely fixed by the relative strength of the λ_1 eigenvalue with respect to the λ_{th}. As we increase/decrease the threshold value λ_{th}, voids increase/decrease progressively through contours of increasing/decreasing λ_1.

Voids are thus characterized by low values of both FA and λ_1. In Fig. 2 we show that the these two values are indeed closely correlated. The left panel shows the correlation between λ_1 and FA for all the grid cells in the simulation while the right panel shows the correlation between λ_1 and the local overdensity δ. This shows that the overdensity has a large scatter at fixed λ_1.

From Figs. 1 and 2 we conclude that the FA is a good tracer of voids as it is almost perfectly correlated with low values of λ_1. We propose that voids should be composed completely by regions of FA< 0.95. If we increase the values of λ_1 from its minimum until it we reach FA$= 0.95$ in 2 we find that this correspond to critical values of $\lambda_1^T = 0.265$ and $\lambda_1^V = 0.175$ for the Tweb and Vweb, respectively. This means that setting λ_{th} to either λ_1^T/λ_1^V automatically produces voids with all the cells $FA < 0.95$. The middle column in Fig. 1 shows the web classification for this choice of λ_{th}, demonstrating that it is a sensible choice to define voids.

4.3 Defining voids with a watershed algorithm

Once established the FA as a good tracer of voids, the next step is to find individuals voids in the overall distribution. For this purpose, we use the *watershed transform algorithm* (Beucher & Lantuejoul 1979; Beucher & Meyer 1993), in which a void is identified as the catching basin of a local minimum of the FA. The use of this algorithm is advantageous as it is parameter-free and does not require any assumption on the shape and morphology of voids.

Previous implementations of this technique as those of Platen et al. (2007); Neyrinck (2008) have shown remarkable results regarding voids finding, however they use the density field instead of the FA field. On the other hand, we use a *cloud-in-cell* (`CIC`) algorithm on a Cartesian mesh for estimating the density and tensor fields, instead of the more sophisticated *Delaunay tessellation for field estimator* (`DTFE`) technique (Schaap & van de Weygaert 2000), but our implementation of the watershed transform should not be significantly affected as we are interested in low density regions where the `CIC` gives similar estimations.

As suggested by Platen et al. (2007) and references therein, it is necessary to apply a threshold merger in order to reduce spurious features and to avoid void hierarchization. A natural choice is a threshold of $\delta = -0.8$, which means that any ridge between two voids with density below that value would be removed and the respective voids merged. As we are working with the FA, the equivalent threshold according to Fig. 2 is $FA = 0.65$. In right panels of Fig. 1 we show the resulting catalogs of voids for both schemes.
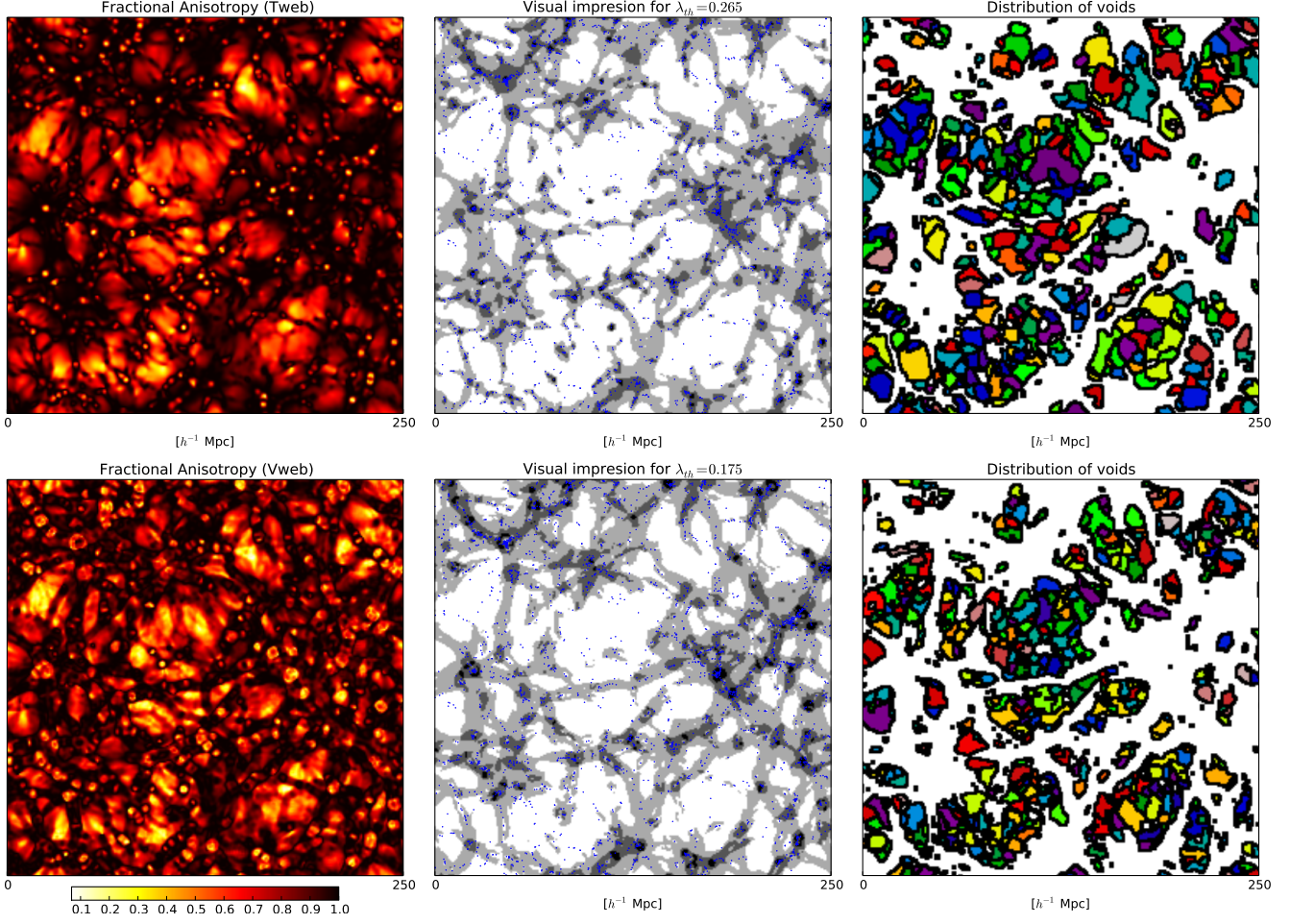
Figure 1. Left colum. Visual impression of the FA field over a slide of the simulation for each web scheme (T-web, upper panels. V-web, middle panels). Middle column. Components of the Cosmic Web using λ_{th} values that put an upper bound of $FA = 0.95$ to voids. Voids corresponds with white, sheets to gray, filaments to dark gray and knots with black regions. Right column. Sketches the distribution of the catalogued voids by our method.
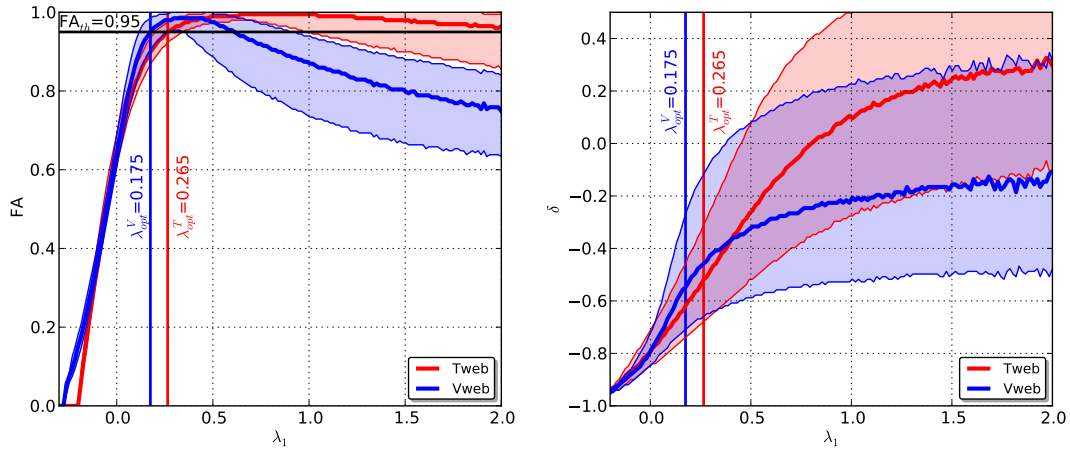

Figure 2. Distributions of the FA (left panel) and the density field (right panel) with respect to the eigenvalue λ_1 for each web scheme (Tweb, red lines. Vweb, blue lines) as calculated over all cells of the grid. Thick central lines correspond with the median and filled regions with the 50% of the distribution.

5 RESULTS

5.1 The void size distribution

5.2 Density profile of voids

$$\mathcal{C} = \frac{M_v}{\overline{M}} = \frac{3}{2R^3} \int_0^R [\delta(r) + 1] r^2 dr$$

$$\mathcal{C} < 1$$

$$\mathcal{C} > 1$$

6 CONCLUSIONS

ACKNOWLEDGMENTS

REFERENCES

Abazajian K., et al. (the SDSS Collaboration) 2003, AJ, 126, 2081

Basser P., 1995, NMR in Biomedical Imaging, 8, 333

Bertschinger E., 1985, ApJS, 58, 1

Beucher S., Lantuejoul C., 1979, in Proceedings International Workshop on Image Processing, CCETT/IRISA, Rennes, France

Beucher S., Meyer F., 1993, Mathematical Morphology in Image Processing. Marcel Deker, New York

Blumenthal G. R., da Costa L. N., Goldwirth D. S., Lecar M., Piran T., 1992, ApJ, 388, 234

Bond J. R., Kofman L., Pogosyan D., 1996, Nature, 380, 603

Brunino R., Trujillo I., Pearce F. R., Thomas P. A., 2007, MNRAS, 375, 184

Ceccarelli L., Padilla N. D., Valotto C., Lambas D. G., 2006, MNRAS, 373, 1440

Ceccarelli L., Paz D., Lares M., Padilla N., Lambas D. G., 2013, MNRAS, 434, 1435

Chincarini G., Rood H. J., 1975, Nature, 257, 294

Colberg J. M., Pearce F., et al. 2008, MNRAS, 387, 933

Colberg J. M., Sheth R. K., Diaferio A., Gao L., Yoshida N., 2005, MNRAS, 360, 216

Colless M., et al. (the 2dFGRS Team), 2001, MNRAS, 328, 1039

Colless M., et al. (the 2dFGRS Team), 2003, VizieR Online Data Catalog, 7226

Croton D. J., et al. 2004, MNRAS, 352, 828

Dubinski J., da Costa L. N., Goldwirth D. S., Lecar M., Piran T., 1993, ApJ, 410, 458

Einasto J., Joeveer M., Saar E., 1980a, MNRAS, 193, 353

Einasto J., Joeveer M., Saar E., 1980b, Nature, 283, 47

Forero-Romero J. E., Contreras S., Padilla N., 2014, MNRAS, 443, 1090

Forero-Romero J. E., Hoffman Y., Gottlöber S., Klypin A., Yepes G., 2009, MNRAS, 396, 1815

Foster C., Nelson L. A., 2009, ApJ, 699, 1252

Gottlöber S., Łokas E. L., Klypin A., Hoffman Y., 2003, MNRAS, 344, 715

Gregory S. A., Thompson L. A., 1978, ApJ, 222, 784

Hahn O., Porciani C., Carollo C. M., Dekel A., 2007, MNRAS, 375, 489

Hoffman Y., Metuki O., Yepes G., Gottlöber S., Forero-Romero J. E., Libeskind N. I., Knebe A., 2012, MNRAS, 425, 2049

Hoffman Y., Shaham J., 1982, ApJL, 262, L23

Hoyle F., Vogeley M. S., 2004, ApJ, 607, 751

Icke V., 1984, MNRAS, 206, 1P

Jarosik N., Bennett C. L., et al. 2011, ApJS, 192, 14

Kauffmann G., Fairall A. P., 1991, MNRAS, 248, 313

Kirshner R. P., Oemler Jr. A., Schechter P. L., Shectman S. A., 1981, ApJL, 248, L57

Kirshner R. P., Oemler Jr. A., Schechter P. L., Shectman S. A., 1987, ApJ, 314, 493

Klypin A. A., Trujillo-Gomez S., Primack J., 2011, ApJ, 740, 102

Libeskind N. I., Hoffman Y., Forero-Romero J., Gottlöber S., Knebe A., Steinmetz M., Klypin A., 2013, MNRAS, 428, 2489

Martel H., Wasserman I., 1990, ApJ, 348, 1

Micheletti D., et al. 2014, ArXiv e-prints

Muñoz-Cuartas J. C., Müller V., Forero-Romero J. E., 2011, MNRAS, 417, 1303

Müller V., Arbabi-Bidgoli S., Einasto J., Tucker D., 2000, MNRAS, 318, 280

Nadathur S., Hotchkiss S., 2014, MNRAS, 440, 1248

Neyrinck M. C., 2008, MNRAS, 386, 2101

Neyrinck M. C., Falck B. L., Szalay A. S., 2013, ArXiv e-prints

Pan D. C., Vogeley M. S., Hoyle F., Choi Y.-Y., Park C., 2012, MNRAS, 421, 926

Patiri S. G., Betancort-Rijo J., Prada F., 2006, MNRAS, 368, 1132

Patiri S. G., Prada F., Holtzman J., Klypin A., Betancort-Rijo J., 2006, MNRAS, 372, 1710

Platen E., van de Weygaert R., Jones B. J. T., 2007, MNRAS, 380, 551

Plionis M., Basilakos S., 2002, MNRAS, 330, 399

Regos E., Geller M. J., 1991, ApJ, 377, 14

Ricciardelli E., Quilis V., Planelles S., 2013, MNRAS, 434, 1192

Riebe K., Partl A. M., Enke H., Forero-Romero J., Gottloeber S., Klypin A., Lemson G., Prada F., Primack J. R., Steinmetz M., Turchaninov V., 2013, Astronomische Nachrichten, 334, 691

Rojas R. R., Vogeley M. S., Hoyle F., Brinkmann J., 2005, ApJ, 624, 571

Schaap W. E., van de Weygaert R., 2000, A&A, 363, L29

Shandarin S., Feldman H. A., Heitmann K., Habib S., 2006, MNRAS, 367, 1629

Sutter P. M., Lavaux G., Hamaus N., Pisani A., Wandelt B. D., Warren M. S., Villaescusa-Navarro F., Zivick P., Mao Q., Thompson B. B., 2014, ArXiv e-prints

Sutter P. M., Lavaux G., Wandelt B. D., Weinberg D. H., 2012, ApJ, 761, 44

Sutter P. M., Lavaux G., Wandelt B. D., Weinberg D. H., Warren M. S., 2014, MNRAS, 438, 3177

Tikhonov A. V., 2006, Astronomy Letters, 32, 727

Tikhonov A. V., 2007, Astronomy Letters, 33, 499

van de Weygaert R., van Kampen E., 1993, MNRAS, 263, 481

von Benda-Beckmann A. M., Müller V., 2008, MNRAS, 384, 1189

York D. G., et al. (the SDSS Collaboration), 2000, AJ, 120, 1579

Zeldovich I. B., Einasto J., Shandarin S. F., 1982, Nature, 300, 407
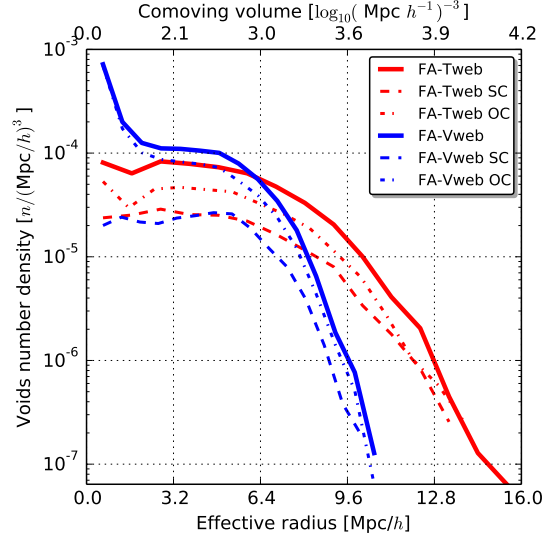
Zel'dovich Y. B., 1970, A&A, 5, 84

Figure 3. Volume functions of voids for both built catalogs. Watershed-Tweb (red curves), Watershed-Vweb (blue curves). Continuous lines corresponds with the total number of voids, dot-dashed with sub-compensated voids and dashed lines with over-compensated voids.
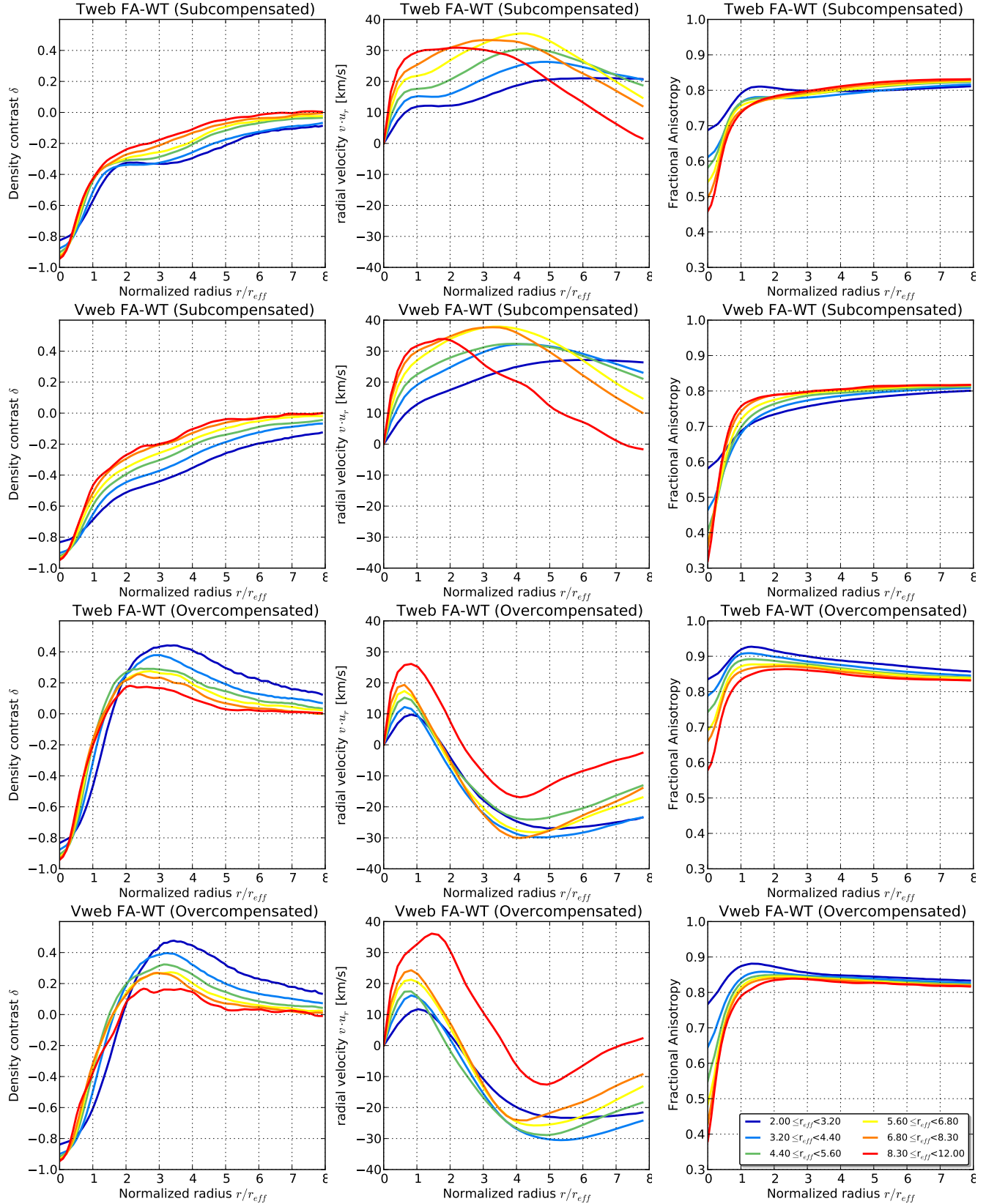
Figure 4. Density of voids for each finding scheme.